Electron-impact detachment from Cl^-

K. Fritioff,[1] J. Sandström,[1] D. Hanstorp,[1] A. Ehlerding,[2] M. Larsson,[2] G. F. Collins,[3] D. J. Pegg,[4] H. Danared, A. Källberg,[5] and A. Le Padellec[6]

[1]*Department of Physics, Chalmers University of Technology/Göteborg University, S-412 96 Göteborg, Sweden*

[2]*Department of Physics, AlbaNova Stockholm University, S-106 91 Stockholm, Sweden*

[3]*Physics Department, Queen's University Belfast, Belfast BT7 1NN, Northern Ireland, United Kingdom*

[4]*Department of Physics, University of Tennessee, Knoxville, Tennessee 37996, USA*

[5]*Manne Siegbahn Laboratory, Frescativägen 24, SE-104 05 Stockholm, Sweden*

[6]*LCAR UMR 5589, Université Paul Sabatier-Toulouse III, 118 route de Narbonne, Bâtiment III R1B4, 31062 Toulouse Cedex 4, France*

(Received 7 February 2003; published 16 July 2003)

Single-, double- and triple-electron-impact detachments from the Cl^- ion have been investigated over a collision energy range of 0–95 eV. The experiment was performed at the ion storage ring CRYRING at the Manne Siegbahn Laboratory. The Cl^- ions, produced in a sputter ion source, were injected into the ring and accelerated to 2.7 MeV. Thereafter the ions were merged with an electron beam. The electrons served to cool the ion beam. Then they were used as a partner in the electron-ion collisions. The products of the detachment processes, Cl atoms, Cl^+, and Cl^{2+} ions, were detected after the interaction region with surface-barrier detectors. The shapes of the cross sections for the single, double, and triple detachments show striking similarities.

DOI: 10.1103/PhysRevA.68.012712 PACS number(s): 34.80.Dp, 34.80.Kw

I. INTRODUCTION

Electron detachment arising from the collision of an electron with a negative ion is a fundamental process. The interelectronic interaction is relatively more important than for positive ions and experimental studies on these systems can serve as sensitive tests for theoretical models. Pioneering work was carried out by Tisone and Branscomb [1], Peart *et al.*, [2] and later by Brouillard and co-worker [3]. These investigators used crossed-beam methods to determine absolute electron-impact detachment cross sections for several different anions. The advent of heavy-ion magnetic storage rings with electron coolers serving as targets has made it possible to measure absolute cross sections for electron detachment following electron impact even from zero collision energy with a very good energy resolution. Electron collisions with both atomic and molecular negative ions have been investigated [4–11] utilizing the storage ring techniques. The ions are accumulated in the ring and make multiple passes through the electron target, thus enhancing reaction rates. Prior to the detachment measurements, the energy spread of the ions is reduced by phase-space cooling via interactions with velocity-matched electrons. This leads to a considerable improvement in the energy resolution of the measurements. Most of the previous measurements involve the detachment of a single electron. In this paper, we report on multiple detachment as well as single detachment.

There is currently a growing database on measured electron-impact detachment cross sections [12]. Calculations of these detachment processes, however, have been far less forthcoming due to difficulties associated with the dynamics of the detachment process [13,14], which involves extensive electron correlation in both the initial and final states of the collision. In the initial state, the incident electron experiences a repulsive long-range Coulomb interaction with the negative ion and an attractive short-range interaction with the core. In the multielectron final state there exist one or more detached electrons, in addition to the scattered electron. In both the initial and final states, the incident electron experiences a Coulomb potential barrier and at low energies tunneling is involved. Correlation is expected to be particularly strong near threshold, since the electrons are receding slowly from the core [15].

In addition to their intrinsic importance in understanding few-particle interactions, negative ions also play an important role in many applications. Negative ions of the halogens, for example, are constituents of low-density plasmas used in material processing [16]. The ability to model such plasmas requires a detailed knowledge of cross sections for the production and destruction of their negative ion constituents by electron impact. We have previously performed one such study involving the electron-impact single-detachment cross section of F^- [17].

In this paper, we present recent measurements of absolute cross sections for the electron-impact detachment of one, two, and three electrons from the Cl^- ion over a range of collision energies from 0 eV to 95 eV. These cross sections will be designated σ_0, σ_+, and σ_{2+}, respectively. Specifically, the following processes have been studied:

$$\begin{aligned} \sigma_0&: \ Cl^- + e^- \rightarrow Cl + 2e^-, \\ \sigma_+&: \ Cl^- + e^- \rightarrow Cl^+ + 3e^-, \\ \sigma_{2+}&: \ Cl^- + e^- \rightarrow Cl^{2+} + 4e^-. \end{aligned} \tag{1}$$

This paper is organized in the following manner. Section II is an overview of the facility and the experimental procedures. Section III is a description of the methods used to analyze the data. In Sec. IV, the experimental results are

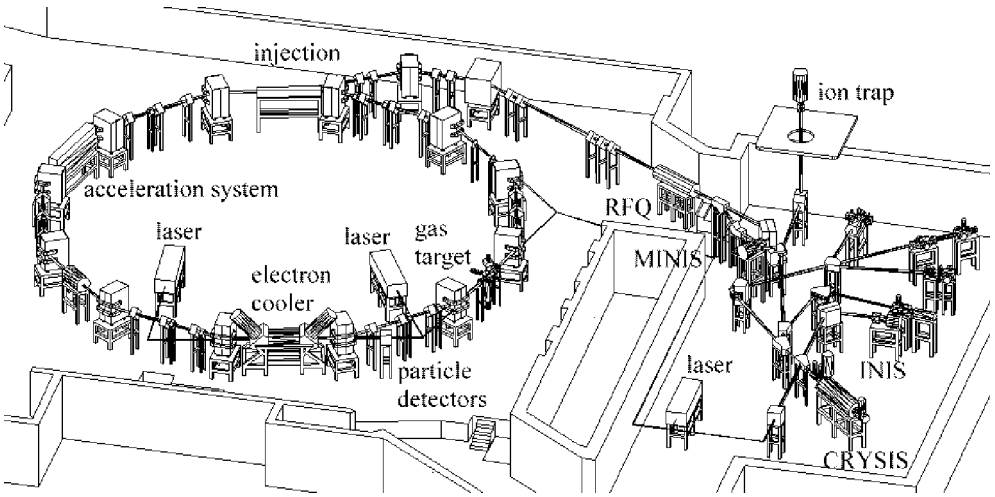

FIG. 1. A schematic diagram of the heavy-ion storage ring CRYRING.

presented and in Sec. V a discussion of the results is given. Finally, in Sec. VI, the results of the experiment are summarized.

II. EXPERIMENT

The experiment was performed at the heavy-ion storage ring CRYRING [18], situated at the Manne Siegbahn Laboratory in Stockholm, Sweden. This facility was originally designed for the storage of highly charged positive ions but has since been used to great effect also in the studies of singly charged ion. Large ion currents can be produced in the ring by a multiturn injection method and electron cooling [19]. The energy resolution in the collision process is significantly improved by the use of phase-space cooling [20]. The experimental facility is shown schematically in Fig. 1.

The Cl^- ions were produced in a cesium sputter ion source [21]. In this type of source, liquid cesium is evaporated in an oven and ionized on a hot anode. The resulting beam of positive cesium ions is then accelerated towards a solid cathode target. The cathode material is chosen to efficiently produce the specie of interest by sputtering. In the present work, AgCl was used. The cesium, in addition to sputtering the cathode material, deposits a few monolayers on the surface of the cathode. Sputtered atoms and molecules leaving the cathode pick up an extra electron from the deposited cesium to form negative ions. The ion current, as measured after a mass-selecting magnet, was typically a few microamperes. After extraction from the source at 40 keV, the ions were injected into the ring and accelerated with a nonresonant driven drift tube. The maximum ion energy is then $96(q/m_{ion})^2$ MeV/amu, where m_{ion} is the ion mass in amu and q is the ion charge state. This value is determined by the magnetic rigidity of the ring. In the present case, the Cl^- ions were accelerated to the maximum allowable energy of 2.7 MeV.

The lifetime of the Cl^- ion beam in the ring was 3.0 s, at a residual-gas pressure lower than 1×10^{-11} mbar. The finite beam lifetime is associated with the fact that the ions can be neutralized in collisions with the background gas, which consists mainly of H_2. After about four lifetimes, the ion current had decreased to a value that was too small to perform an experiment, and the beam was dumped. In our case, each experimental cycle, therefore, lasted 12 s. The ring cycle consisted of five stages: injection, acceleration, cooling, measurement, and dumping of the beam. The time dependence of the data accumulation is shown in Fig. 2.

During the cooling period, the ions interacted with velocity-matched electrons in the electron cooler in a collinear geometry. The electron beam is adiabatically expanded by the decreasing field between the superconducting magnet surrounding the electron gun (<3 T) and the field in the magnets which guide the electrons through the cooler ($=0.03$ T). This expansion reduces the transverse electron temperature [22]. The transverse and longitudinal electron temperatures in this particular experiment were 8 meV and 0.05 meV, respectively. The Coulomb interaction between

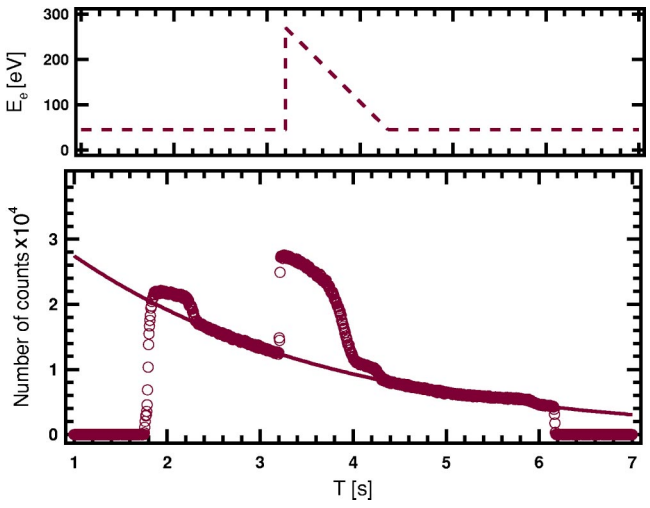

FIG. 2. The dashed curve in the top figure represents the electron energy in the laboratory frame as a function of the time after injection. The open circles in the figure at the bottom show a typical count rate on the SBD. The solid line is a curve fit to the data in the regions where the electron cooler was turned off.

the ions and the cold electrons causes a reduction in the thermal random motion of the ions. This is called phase-space cooling. At this stage, the collision energies were insufficient to detach the extra electron from the Cl^- ion. After the ions had been cooled, the electron velocity was detuned from the velocity-matched condition in order to create a finite collision energy in the center-of-mass frame, E_{cm}, given by

$$E_{cm}=(\sqrt{E_e}-\sqrt{E_{cool}})^2, \tag{2}$$

where E_e is the average electron energy in the laboratory frame and E_{cool} is the electron cooling energy, i.e., the energy of the electrons at the cooling condition when the electrons and ions have the same average velocity. In this expression, the reduced mass of the electron and ion is approximated with the mass of the electron. Furthermore, the threshold energy in the center-of-mass frame for the detachment reaction is much larger than the temperature of the electrons. The center-of-mass collision velocity is, therefore, taken to be the same as the detuning velocity, omitting the electron temperature. The drag force between the electrons and the ions is considered to be negligible in this case. For a beam of Cl^- ions at the full energy of 2.7 MeV, the electron cooling energy is 45 eV in the laboratory frame. In the present experiment, we used collision energies E_{cm} ranging from zero to 95 eV.

Neutral and positively charged Cl fragments originating from the detachment processes were detected after they emerged from the interaction region. Cl atoms were produced either from electron-impact-induced single detachment or from collisions with the background gas. These neutral particles, unaffected by the magnetic field of the dipole magnets of the ring, followed their original trajectory and emerged along a tangential path. They then impinged on an energy sensitive surface-barrier detector (SBD), which was placed in the zero-degree arm at a distance 3.5 m downstream from the interaction region. The positive fragments Cl^+ and Cl^{2+} were deflected out of the beam by the dipole magnet along different trajectories due to their charge state differences. A movable surface-barrier detector was used in this case. The signals from this SBD and the one used to monitor the production of Cl fragments were recorded using multichannel scalers.

The magnitude of the ion current in the ring had to be determined accurately in order to establish an absolute scale for the cross sections. This was measured by the use of a dc transformer to be 0.055 mA directly after the acceleration. The ion current had to be determined separately from the other measurements due to the fact that the operation of the transformer required an ion current so large that it would have saturated the SBD. All the measurements were then normalized using the output of a scintillation detector. This detector was capable of handling the destruction rate of the ions over a large dynamic range. The scintillation detector was placed in the zero-degree direction in another section of the ring. The absolute cross section was determined by first relating the destruction rate measured by the SBD to the signal from the scintillation detector. The signal from the scintillation detector was then related to the absolute ion current measurement recorded with the dc transformer.

III. DATA ANALYSIS

In this section, the general principles of how the experimental raw data were transformed into cross sections will be described. This includes a discussion of how the data are corrected both for space charge and for the effects related to the merging of the electrons with the ions in the cooler region.

The open circles in Fig. 2 show the total count rate on the SBD for the single-detachment process as a function of the time T after the ions were injected into the ring. The recording of the signal started at $T=1.8$ s when a flag in front of the detector was opened. By this time, the ions already had been accelerated to full energy. The cooling occurred in the interval $T=1.1$–2.4 s. In the interval $T=2.4$–3.2 s, the electrons are turned off. The decrease in the signal that occurs when the electrons at the cooling energy are turned off indicates that positive ions are trapped by the electron beam in the cooler prior to this time. Collisions between the trapped positive ions, mostly H_2^+, and the negative ions in the ring produce neutral fragments that are detected. This contribution to the background disappears when the electron beam is turned off. At $T=3.2$ s, the electron beam is turned on again and the collision energy is ramped from 95 eV down to 0 eV in 1 s. The knee observed in the figure at $T=4$ s corresponds to the threshold for the electron-impact single-detachment process. At $T=4.2$ s the electron beam is turned off and at $T=6.2$ s the flag in front of the detector is closed again.

In the analysis, we define the measured count rate R_{meas} as the sum of the rates for detachment due to collisions with electrons in the cooler, R_{signal}, and for collisions with background gas in the same ring section, R_{bg}. The time dependence in all the expressions is omitted for clarity. The cross section σ is related to R_{signal} according to

$$R_{signal}=N_{ion}\frac{ln_e}{C}\langle v\sigma\rangle, \tag{3}$$

where N_{ion} is the total number of ions stored in the ring, l is the length of the region where the electron and ion beams are parallel (the interaction region), n_e is the electron density, and C is the circumference of the ring. v is the relative velocity between the ions, v_{ion}, and the electrons, v_e, e.g., $v=|\overline{v_e}-\overline{v_{ion}}|$. The expression $\langle v\sigma\rangle$ in the equation indicates that the cross section, in principle, has to be convoluted with the electron velocity distribution, $f(v_e)$ [20],

$$\langle v\sigma\rangle=\int f(v_e)\sigma(v)v\,d^3v_e, \tag{4}$$

where

$$f(v_e)=\frac{m_e}{2\pi kT_{e\perp}}\left(\frac{m_e}{2\pi kT_{e\parallel}}\right)^{1/2}\exp\left(-\frac{m_e v_{e\perp}^2}{2kT_{e\perp}}-\frac{m_e v_{e\parallel}^2}{2kTe\parallel}\right). \tag{5}$$

The quantity v_e is the electron velocity in the laboratory frame, m_e is the mass of the electron, $v_{e\perp}$ and $v_{e\|}$ are the electron velocities due to the electron temperature, k is the Boltzmann constant, and $T_{e\perp/\|}$ are the parallel and perpendicular electron temperatures, respectively. It is customary to call $\langle v\sigma\rangle$ the rate coefficient. In this measurement, the collision energies for nonzero cross sections are relatively large. The temperature of the electrons are, therefore, negligible. This allows us to make the assumption that the relative velocity v is equal to the detuning velocity, $v_d=|v_e-v_{ion}|$ and $\langle v\sigma\rangle=v\sigma$.

R_{signal} is obtained by subtracting the exponentially decaying background rate R_{bg} shown as a solid curve in Fig. 2, from the total measured count rate R_{meas}. The quantity R_{bg} is determined from an interpolation of a curve fit to the data points accumulated before and after the electron ramp, when there are no electrons interacting with the ions. The total number of ions in the ring during the electron detachment measurement, N_{ion}, is derived from the measured neutralization rate on the scintillator detector, R_N, acquired at the same time. The normalized destruction rate $R_B=R_N/N_{ion}$ is the same during the detachment measurement as during the current measurement. In the latter case, R_B can also be written as

$$R_B=\frac{R_{N'}}{I_{ion}}\frac{v_{ion}e}{C}. \tag{6}$$

Here, $R_{N'}$ is the neutralization rate measured with the scintillation detector during the ion current measurement, I_{ion} is the ion current, and v_{ion} is the velocity of the ions in the laboratory frame. The cross section, written in terms of the measurable quantities, can be expressed as

$$\sigma=R_B\frac{C}{n_e v l}\frac{R_{meas}-R_{bg}}{R_N}. \tag{7}$$

The electrons in the cooler will not reach the energy corresponding to the potential on the anode of the cooler due to the space-charge potential produced by the electrons themselves. This space-charge potential V_{sp} can be calculated using the Poisson equation $\nabla^2 V_{sp}(r)=-\rho(r)/\epsilon_0$, where $\rho(r)$ is the electron density at radial distance r from the center of the electron beam. The space-charge potential in the electron beam can be expressed as

$$V_{sp}=\rho(r)\frac{r_e^2}{2\epsilon_0}\left[0.5+\ln\left(\frac{r_{ch}}{r_e}\right)\right]. \tag{8}$$

In the equation, r_e is the radius of the electron beam and r_{ch} is the radius of the vacuum chamber. The space-charge effect caused by the electrons in the cooler will be compensated, to some extent, by positively charged rest gas ions trapped in the potential well produced by the electrons. These trapped positive ions, mostly H_2^+, will partially neutralize the space charge and therefore diminish the predicted change in electron energy. The magnitude of this neutralization effect is estimated at the cooling condition when the electron velocity is equal to the ion velocity. The real electron energy can then be calculated from the velocity of the ions, $E_e=m_e v_{ion}^2/2$. At cooling, the electron energy can be expressed as

$$E_e=E_{cool}-(1-d)eV_{sp}, \tag{9}$$

where E_{cool} is the electron energy at cooling as read on the power supply connected to the electron gun at cooling and d is a value of the neutralization effect. For other collision energies, tabulated values of the cross section for production of H_2^+ are used to scale the neutralization effect and derive the correct electron energy. As a result of this effect, the electron energy is uniformly decreased by about 1.6 eV throughout the whole range of the collision energies.

Another important thing to consider in the analysis of the cross section is that the electron beam is bent in and out of the ion beam in the electron cooler by two toroidal magnets. Detachment events from these regions will contribute significantly to the signal on the SBDs. The collision energy, however, will be larger than that in the collinear part of the cooler defined by the electron and ion beams. A correction must be made by subtracting the additional signal due to this toroidal effect. The real collision energy $E(x,E_{cm})$ is calculated as a function of the position x in the electron cooler and the nominal collision energy E_{cm}. The rate coefficient $\alpha(E_{cm})=\langle v\sigma\rangle$ can be expressed in terms of the measured rate coefficient $\alpha_{meas}(E_{cm})$ minus a correction term $\Delta\alpha(E_{cm})$ caused by the toroidal effect,

$$\alpha(E_{cm})=\alpha_{meas}(E_{cm})-\Delta\alpha(E_{cm}). \tag{10}$$

The correction can be written as

$$\Delta\alpha(E_{cm})=l^{-1}\int \alpha(E(x,E_{cm}))dx-\alpha(E_{cm}), \tag{11}$$

where the integration extends over the complete overlap region in the cooler. $\alpha(E_{cm})$ is obtained from an iterative procedure involving Eqs. (10) and (11) by initially setting $\alpha(E_{cm})=\alpha_{meas}(E_{cm})$. This correction reduced the cross section by approximately 30% at all energies. This significant correction is not unexpected since the toroidal regions have a total length of 40 cm, which is an appreciable fraction of the interaction length of 85 cm defined by the parallel beams.

IV. RESULTS

Detachment arising from electron impact on the Cl^- ion has been investigated over the collision energy range, 0–95 eV. Single-, double-, and triple-electron detachment cross sections have been measured and the results are presented in this section. The error bars shown on selected cross-section data points in Fig. 5 represent the square root of the number of counts in each data point. In Figs. 3 and 4, the corresponding error bars are smaller than the circles representing the data points.

Figure 3 shows the cross section σ_0 for the electron-impact single detachment from Cl^- in the energy range 0 eV–95 eV. In this process, the incident electron detaches a valence electron from Cl^-, leaving a neutral Cl atom in its ground state:

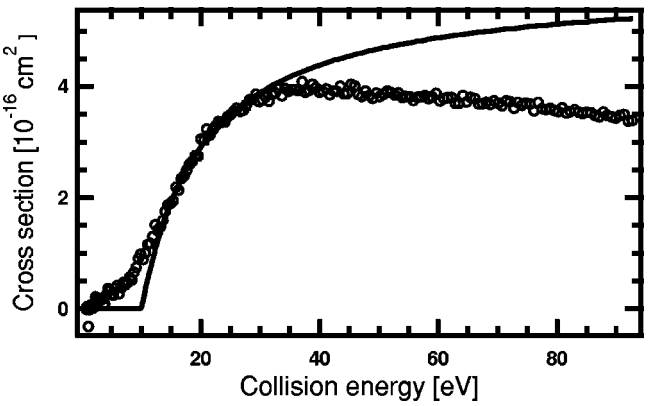

FIG. 3. The data points (open circles) represent the single-electron detachment cross section for electron impact on Cl^-. The solid line is a fit to the data using the OTB model in the energy range 10–30 eV (see Sec. V).

$$Cl^-(3p^6\,{}^1S_0)+e^-(\epsilon)\rightarrow Cl(3p^5\,{}^2P_{3/2})+2e^-(\epsilon). \quad (12)$$

This process has a threshold according to the over-the-barrier (OTB) model around 10 eV. The OTB model is discussed in Sec. V. The cross section increases monotonically from zero up to a maximum of $3.97(42)\times10^{-16}$ cm^2 at 40 eV. It then decreases linearly up to the largest measured energy of 95 eV. The electron affinity (EA) of Cl is 3.6 eV [23]. The first excited state in chlorine, $Cl^*(3p^4 4s\,{}^3P)$, has an excitation energy of 8.9 eV [24]. The threshold for the reaction involving this state would then be at 3.6 eV + 8.9 eV = 12.5 eV. Energetically this threshold is attainable, but we do not observe any structure in the cross-section curve at this energy. We, therefore, conclude that the residual Cl atom is left only in its ground state. The rise in the cross section prior to the model threshold most likely arises from tunneling events.

Figure 4 shows the cross section σ_+ for the electron impact double detachment:

$$Cl^-(3p^6\,{}^1S_0)+e^-(\epsilon)\rightarrow Cl^+(3p^4\,{}^3P_2)+3e^-(\epsilon). \quad (13)$$

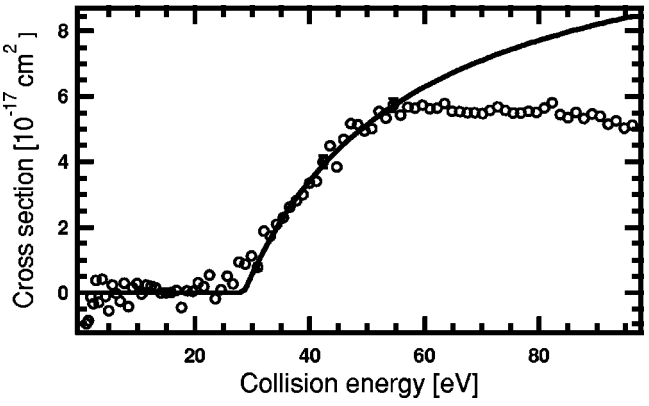

FIG. 4. The data points show the double-electron detachment cross section of electron impact on Cl^-. The solid line is a fit to the data using the OTB model over the energy range 33–50 eV (see Sec. V).

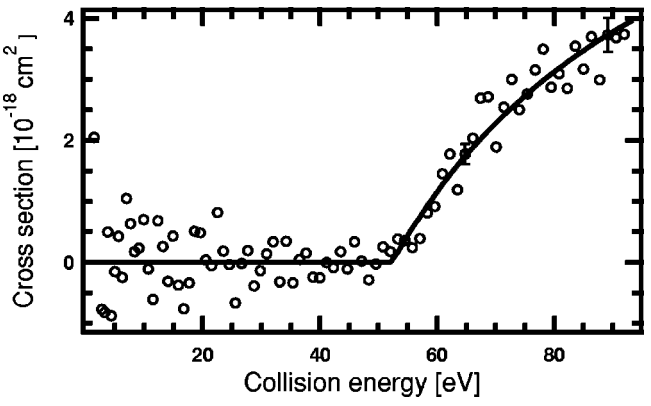

FIG. 5. The data points show the triple-electron detachment cross section for electron impact on Cl^-. The solid line is a fit to the data using the OTB model over the energy range 55–90 eV (see Sec. V).

The same argument cited in the case of the single detachment can be used to show that the residual Cl^+ ions are formed in their ground state at all collision energies. The cross section increases monotonically to a maximum value of $5.7(6)\times10^{-17}$ cm^2 at 60 eV. It then decreases linearly up to the maximum measured collision energy of 95 eV.

For even higher collision energies, the incoming electron can detach three electrons:

$$Cl^-(3p^6\,{}^1S_0)+e^-(\epsilon)\rightarrow Cl^{2+}(3p^3\,{}^4S_{3/2})+4e^-(\epsilon). \quad (14)$$

The cross section σ_{2+} for this reaction is presented in Fig. 5. The reaction starts at 52.3 eV and rises monotonically to a value of 4.1×10^{-18} cm^2 at the highest measured collision energy.

In Table I, we summarize the experimental results by presenting the measured threshold energies together with the energies and magnitudes for the maximum cross section for each of the curves. For σ_0, the total binding energy refers to the electron affinity of Cl. In the case of σ_+, it indicates the sum of the EA of Cl^- and the ionization potential of Cl (13.0 eV [25]). In the case of σ_{2+}, it represents the sum of the EA and the ionization potentials of Cl^+ and Cl^{2+}, which is 23.8 eV [25]. The measured threshold energies are obtained by extrapolating an OTB model fit, as described in Sec. V.

The statistical uncertainties in the cross sections quoted in our results originate from the signals produced by the surface-barrier detectors, the scintillation detector, and from

TABLE I. The maximum cross section σ_{max} for the single-, double-, and triple-detachment processes. The error in the maximum cross-section value is the total statistical uncertainty at the 1σ level.

	Total binding energy (eV)	Threshold energy (eV)	σ_{max} (10^{-16} cm^2)	$E_{\sigma_{max}}$ (eV)
σ_0	3.6	10.1	3.97(42)	40
σ_+	16.6	28.6	0.57(6)	60
σ_{2+}	40.4	52.3		

the ion current measurement. It is, however, only the square root of the number of counts in the SBD signals that will contribute to the scatter in the final cross-section data. The error bars shown in Fig. 5, therefore, represent only the statistical uncertainties in the SBD signals. In Figs. 3 and 4, the corresponding error bars are smaller than the circles representing the data points. In the analysis of the cross section, the signals from the scintillation detector and from the current transformer were fitted to exponential curves. The statistical fluctuations yielded an uncertainty in the fitting parameters. This contributes with an additional statistical uncertainty of 9% and 7% at the maximum of the cross section for the single and double detachments, respectively. The corresponding uncertainty in the case of the triple detachment is 12% at the maximum measured energy.

The dominant contribution to the systematic uncertainty arises from the measurement of the ion current (10%) and the length of the interaction region (5%). In addition, there is an uncertainty in the electron current (2%), the radius of the electron beam (1%), the circumference of the storage ring (0.5%), and in the revolution frequency of the ions ($<0.01\%$). The toroidal correction contributes to the total uncertainty with 2%. Combining all these independent uncertainties quadratically yields an estimated overall systematic uncertainty of 12%. The detection efficiency is unity for both the SBD detectors.

The knowledge of the collision energy is limited by the uncertainty in the estimation of the effect of the space charge. The space charge depends on the electron density. In the calculation of the density, one needs to know the electron current, the radius of the electron beam, and the electron velocity. In addition, the uncertainty in the determination of the cooling energy has to be considered. This will affect the whole energy scale, since the zero on this scale is determined when cooling occurs. Furthermore, the nominal electron energy may differ from the energy defined by the power supply due to the presence of contact potentials. An estimation of all these uncertainties adds up to 0.12, 0.18, and 0.23 eV at the threshold energies for the single, double, triple detachments, respectively.

The temperature of the electron beam and the ion beam ultimately determines the energy resolution. Since the ions are much heavier than the electrons, the ion velocity spread does not significantly contribute to the energy resolution. A comprehensive treatment of the energy resolution is made by Neau [26]. In the present experiment, however, we do not need the very high resolution, since the cross section varies smoothly over the whole energy range. Therefore, we collect the data in time bins of 5 ms. The change in the collision energy during this dwell time results in an effective experimental energy resolution of 0.35 eV at the threshold for the single detachment and 0.71 eV at the end of the energy ramp. For the double and triple detachments, we used a longer dwell time to accumulate better statistics and the energy resolution is correspondingly worse in these cases. It is estimated to be 1.08 eV at the threshold for the double detachment and 1.25 eV at the threshold for the triple detachment. In both cases, it is 1.40 eV at the end of the ramp.

V. DISCUSSION

In order to determine the threshold energy, it was necessary to apply a model equation that can be fitted to the experimental data. For this purpose, we use a simple classical model developed by Pedersen *et al.* [6]. This OTB model can be used to characterize the single-detachment cross section in the vicinity of the reaction threshold. It makes use of the impact-parameter formalism in which the cross section at a given collision energy E_{cm} can be written as

$$\sigma(E)=2\pi\int_0^\infty P(E_{cm},a)ada, \tag{15}$$

where a is the impact parameter and P is the probability for the reaction to occur. In this model, the probability is represented by a square distribution. If a certain reaction condition is fulfilled, then the probability is p, otherwise it is zero. The reaction takes place only if the kinetic energy of the incoming electron exceeds the electron affinity of the target atom plus the Coulomb energy lost by the electron at some characteristic distance r_{th}. This energy arises from the Coulomb repulsion between the incident electron and the negative ion plus the centrifugal energy. Using this condition in Eq. (15) allows us to write the cross section as

$$\sigma(E)=p\pi r_{th}^2\left(1-\frac{E_{th}}{E_{cm}}\right). \tag{16}$$

Similarly, the threshold for the reaction can be written as

$$E_{th}=EA+\frac{1}{r_{th}}. \tag{17}$$

In reality, however, a reaction can take place at energies below the predicted threshold energy as a result of tunneling. The measured cross section is not exactly zero at the model-dependent threshold, but instead a tail is observed at subthreshold energies. The OTB model can, therefore, only be applied in a region starting sufficiently above the observed threshold so that tunneling can be neglected and ending before the maximum cross section has been reached.

The solid line in Fig. 3 illustrates how the OTB model has been fitted to the experimental results for the single-detachment process. The curve fit was made over the range 13–30 eV. From this fit, we obtain a model threshold value for the reaction of 10.1 eV. The EA of Cl is 3.6 eV [23]. The additional collision energy needed to overcome the repulsive Coulomb barrier between the electron and the negative ion is, therefore, 6.5 eV. The model threshold energy for the reaction is 2.8 times larger than the binding energy. This is in direct contrast to the situation of electron impact on positive ions, where the Coulomb attraction produces a strong signal at zero collision energy. The extra energy needed to overcome the Coulomb repulsion in the case of the detachment of a negative ion is typically slightly more than twice the electron affinity [6].

From the OTB model, the probability for the single-detachment reaction is $p=0.86$ if the incoming electron is closer than 4.3 a.u. from the anion. The calculated radius of

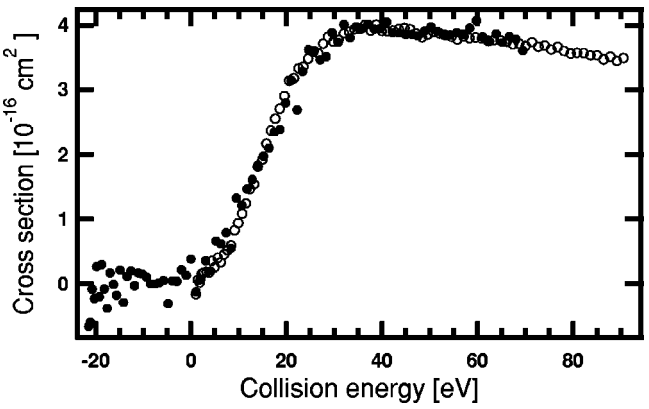

FIG. 6. The open circles show the single-detachment cross section of Cl^- by electron impact. The filled circles are the double-detachment cross section scaled by a factor of 7. The energy scale for the double-detachment curve is shifted down by 22.5 eV in order to have the two detachment curves to coincide in energy.

a Cl atom is 1.84 a.u. [27]. Hence, this simple analysis confirms the well-known fact that a negative ion, with its loosely bound outermost electron, is substantially more spatially extended than the corresponding neutral atom.

The aforementioned classical OTB model is not necessarily applicable to multiple-electron detachment but it seems to fit the cross-section data reasonably well over a limited range and can provide some indication of the location of the thresholds. We performed such a fit to the data resulting from the double-detachment process, which is presented in Fig. 4. In this case, we chose to fit the data in the range 33–51 eV. The threshold energy determined from this fit is 28.6 eV. In the same way, a fit of the OTB model to the triple-detachment data over the energy range 55–90 eV yields a threshold energy of 52.3 eV.

One rather remarkable observation is that the shapes of the single, double, and triple cross sections are essentially the same. Figure 6 shows the cross section for the single and double detachments. The two curves have been normalized so that their thresholds and peak cross sections coincide. The energy scale for the double-detachment curve is shifted down by 22.5 eV in order for the two cross sections to overlap in energy. The magnitude of the cross section for the double detachment is scaled up by a factor of 7. The similarity in shape of the two curves is striking. In addition, the triple-detachment cross-section curve has the same shape as the other two up to the maximum energy that was studied.

One possible explanation of this rather unusual behavior is that the final energy of the scattered electron is essentially the same for all three processes, even though the incident electron energies are different. The scattered electron loses different amounts of energy in the interaction region due to the different energetics associated with each process but it appears to experience the same barrier potential exiting the interaction region as it did entering it. One should also expect a spread in the final velocity of the incident electron due to the inherent momentum spread of the bound electrons in the ion. Thus, some of the electrons will have energies above the barrier height and some below it. The similar shapes of the cross-section curves seem to be determined predominantly by the barrier transmission probability for the scattered electrons, which is the same for the single, double, and triple detachments.

The relative magnitudes of the cross sections, however, are determined by the details of what goes on in the interaction region, seemingly after the incident electron has deposited energy and passed through. Correlation between the six equivalent $3p$ electrons in the closed subshell of Cl^- must surely play an important role in the interaction. The interaction between the incident electron and a single $3p$ electron in the Cl^- ion, for example, probably determines the shape of the single-detachment cross section. The peak in this cross section occurs when the incident electron and the electron bound to the ion are velocity matched. Multiple detachment may then follow from correlated shake-up processes initiated by the detachment of the first $3p$ electron of the Cl^- ion.

VI. SUMMARY

The processes of the single-, double-, and triple-electron-impact detachments from the Cl^- ion have been investigated in a merged beam experiment at the ion storage ring CRYRING. Absolute cross sections were measured over a collision energy range of 0–95 eV. The threshold energies were found to be 10.1, 28.6, and 52.3 eV, respectively. The maximum values of the cross sections were $3.97(42)\times10^{-16}$ cm^{-2} and $0.57(6)\times10^{-16}$ cm^{-2} for the single and double detachments at 40 and 60 eV, respectively. Our measurements on the triple-detachment cross section were below the maximum. A striking similarity of the shapes of the detachment cross sections was found.

ACKNOWLEDGMENTS

This work was supported by the Swedish Research Council (VR) and partly by the European Community's Research Training Networks Program under Contract No. HPRN-CT-2000-0142. A.E. was supported by the EOARD under Contract No. F61775-01-WE035. We thank the staff of the Manne Siegbahn Laboratory for their invaluable help and use of the heavy ion storage ring facility.

[1] G. Tisone and L.M. Branscomb, Phys. Rev. Lett. **17**, 238 (1966).

[2] B. Peart, D.S. Walton, and K.T. Dolder, J. Phys. B: At., Mol. Opt. Phys. **3**, 1346 (1970).

[3] P. Defrance, W. Claeys, and F. Brouillard, J. Phys. B: At., Mol. Opt. Phys. **15**, 3509 (1982).

[4] L. Vejby-Christensen, D. Kella, D. Mathur, H.B. Pedersen, H.T. Schmidt, and L.H. Andersen, Phys. Rev. A **53**, 2371 (1996).

[5] L.H. Andersen, M.J. Jensen, H.B. Pedersen, L. Vejby-

Christensen, and N. Djurić, Phys. Rev. A **58**, 2819 (1998).
[6] H.B. Pedersen, N. Djurić, M.J. Jensen, D. Kella, C.P. Safvan, H.T. Schmidt, L. Vejby-Christensen, and L.H. Andersen, Phys. Rev. A **60**, 2882 (1999).
[7] L.H. Andersen, R. Bilodeau, M.J. Jensen, S.B. Nielsen, C.P. Safvan, and K. Seiersen, J. Chem. Phys. **114**, 147 (2001).
[8] H.B. Pedersen, R. Bilodeau, M.J. Jensen, I.V. Makassiouk, C.P. Safvan, and L.H. Andersen, Phys. Rev. A **63**, 032718 (2001).
[9] A. Le Padellec, K. Andersson, D. Hanstorp, F. Hellberg, M. Larsson, A. Neau, S. Rosén, H.T. Schmidt, R. Thomas, J. Semaniak, D. Pegg, F. Österdahl, H. Danared, and A. Källberg, Phys. Scr. T **64**, 467 (2001).
[10] A. Le Padellec, F. Rabilloud, D. Pegg, A. Neau, F. Hellberg, R. Thomas, H.T. Schmidt, M. Larsson, H. Danared, A. Källberg, K. Andersson, and D. Hanstorp, J. Chem. Phys. **115**, 10671 (2001).
[11] A. Le Padellec, G.F. Collins, H. Danared, A. Källberg, F. Hellberg, A. Neau, K. Fritioff, D. Hanstorp, and M. Larsson, J. Phys. B **35**, 3669 (2002).
[12] H. Tawara and V.P. Shevelko, Int. J. Mass. Spectrom. **192**, 75 (1999).
[13] F. Robicheaux, Phys. Rev. Lett. **82**, 707 (1999).
[14] J.M. Rost, Phys. Rev. Lett. **82**, 1652 (1999).
[15] F. Robicheaux, Phys. Rev. A **60**, 1206 (1999).
[16] W.M. Huo and Y.-K. Kim, IEEE Trans. Plasma Sci. **27**, 1225 (1999).
[17] K. Andersson, D. Hanstorp, A. Neau, S. Rosén, H.T. Schmidt, R. Thomas, M. Larsson, J. Semaniak, F. Österdahl, H. Danared, A. Källberg, and A. Le Padellec, Eur. Phys. J. D **13**, 323 (2001).
[18] K. Abrahamsson, G. Andler, L. Bagge, E. Beebe, P. Carlé, H. Danared, S. Egnell, K. Ehrnstén, M. Engström, C.J. Herrlander, J. Hilke, J. Jeansson, A. Källberg, S. Leontein, L. Liljeby, A. Nilsson, A. Paél, K.G. Rensfelt, U. Rosengård, A. Simonsson, A. Soltan, J. Starker, and M. af Ugglas, Nucl. Instrum. Methods Phys. Res. B **79**, 269 (1993).
[19] H. Poth, Phys. Rep. **196**, 135 (1990).
[20] H. Danared, Nucl. Instrum. Methods Phys. Res. A **391**, 24 (1997).
[21] R. Middleton, Nucl. Instrum. Methods Phys. Res. **214**, 139 (1983).
[22] H. Danared, A. Källberg, G. Andler, L. Bagge, F. Österdahl, A. Paál, K.-G. Rensfelt, A. Simonsson, Ö. Skeppstedt, and M. af Ugglas, Nucl. Instrum. Methods Phys. Res. A **441**, 123 (2000).
[23] U. Berzinsh, M. Gustafsson, D. Hanstorp, A. Klinkmüller, U. Ljungblad, and A.M. Mårtensson-Pendrill, Phys. Rev. A **51**, 231 (1995).
[24] C. Moore, *Atomic Energy Levels*, Natl. Bur. Stand. Ref. Data Ser., Natl. Bur. Stand. (U.S.) Circ. No. 35 (U.S. GPO, Washington, D.C., 1971), Vol. 1, p. 195.
[25] R.L. Kelly, J. Phys. Chem. Ref. Data **16**, Supplement No. 1 (1987).
[26] A. Neau, Ph.D. thesis, Stockholm University, 2002.
[27] C. Froese-Fischer, *The Hartree-Fock Methods for Atoms* (Wiley, New York, 1977), p. 33.